Korean J. Chem. Eng., 34(11), 2823-2831 (2017)
DOI: 10.1007/s11814-017-0182-2

pISSN: 0256-1115
eISSN: 1975-7220

Dry reforming of methane over Ni/SBA-15 catalysts prepared by homogeneous precipitation method

Qiulin Zhang†, Jing Wang, Ping Ning, Tengfei Zhang, Mingzhi Wang, Kaixian Long, and Jianhong Huang

Faculty of Environmental Science and Engineering, Kunming University of Science and Technology, Kunming 650500, P. R. China

(*Received 4 February 2017 • accepted 2 July 2017*)

Abstract−Ni/SBA-15 catalyst was prepared by homogeneous precipitation method (Ni-HP) and used for dry reforming of methane (DRM). The related characterization results indicated that the Ni particles were highly dispersed with a size range of 2-5 nm. Compared with Ni/SBA-15 catalyst prepared by impregnation (Ni-IM), the reduction temperature of Ni-HP obtained from H_2-TPR was greatly improved, suggesting the stronger metal-support interaction. After reacting at 700 °C for 100 h, the CH_4 conversion of DRM over Ni-HP catalyst slightly decreased from 74.5% to 73.8%. While, for the Ni-IM catalyst, the CH_4 conversion dropped from 61.7% to 37.3%. Furthermore, the average particle size of Ni-HP was 3.7 nm and 4.7 nm before and after the long-time stability test, respectively, ascribed to the good anti-sintering property. Although a certain amount of coke was produced, mainly with disorder filamentous carbon of base-growth, the Ni/SBA-15 prepared by homogeneous precipitation exhibited excellent catalytic activity and stability.

Keywords: Dry Reforming, Methane, Ni/SBA-15, Homogeneous Precipitation, Catalyst

INTRODUCTION

Methane shows potential exploitability as clean energy in natural gas. Meanwhile, the efficient transformation of produced CO_2 to valuable source has been investigated intensively. Thereby, the dry reforming of methane (DRM) is an undoubtedly good choice to combine these two aspects, which produces syngas and significantly relieves global warming through utilizing two main greenhouse gases (CH_4 and CO_2) at the same time [1]. Moreover, the ratio of H_2/CO (syngas) is close to 1, so that it can be directly used as the raw material to synthesize the carbonyl or for Fischer-Tropsch synthesis [2,3]. In recent decades, many studies have been undertaken on DRM reaction and preeminent achievements have resulted [4,5]. However, one major drawback of this process is the deactivation of catalyst, resulting from the carbon deposition and the sintering caused by the poor thermal stability [6,7].

It is reported that most transition metals in VIII subunit possess catalytic activity in DRM. Ru, Rh, Pd and Pt, noble metal catalysts, exhibit high catalytic performance and good property to suppress coke formation. However, it is difficult to apply them in large scale industrial practice due to the high price and the limited resource [3,8]. Non-noble metal catalysts such as Ni, Co, Fe and Cu are widely concerned for promising prospect and high value of research in view of their good catalytic activity with low cost. Among them, Ni shows the comparable DRM catalytic performance as noble metals, but its problem of quick deactivation exists because the DRM is a kind of intense endothermic reaction with harsh conditions that require the catalyst to have high thermostability [9,10]. Herein, to effectively improve the properties of Ni-based catalyst to resist carbon formation and sintering has become the present research issue.

According to former reports, the catalytic performance and stability of Ni-based catalysts can be availably improved by the featured support, modified preparation method, introduction of rare earth or alkali metal and addition of noble metal promoters [3,7, 11-13]. Gong et al. [14] adopted nanorod-shaped $La_2O_2CO_3$ as support precursor to disperse and stabilize Ni species with enhanced interaction between Ni and La_2O_3 for DRM. Wang et al. [15] prepared a series of Ni-Co-CaO-ZrO_2 catalysts by a template-free refluxing co-precipitation method to apply in DRM and revealed that the metal synergy effect could promote the activity and stability of catalysts. Liu et al. [16] obtained extremely small Ni particles on the KIT-6 support and strong interaction of Ni with silica matrix by one-spot co-assembly method, which effectively restrains active metal sintering and carbon deposition during the lifetime test of DRM. These strategies are put forward to achieve the advantageous properties of high dispersion, small particle size and strong metal-support interaction, which are crucial to durable catalysts in DRM reaction.

In some ways, to adopt a suitable preparation may be the most direct way to acquire catalysts with the expected properties. As we know, the commonly used impregnation method is an easy and convenient way to prepare supported catalysts. Nevertheless, the attained catalytic performance is undesired in that the Ni species easily aggregate at high temperature and the interaction between support and metal is relatively weak [7,12,17]. Therefore, the apparent disadvantages are not easy to avoid even though it has a good practical simplicity. Recently, many researchers have successfully prepared remarkable Ni-based catalysts for DRM with various methods. Zhang et al. [18] found that a sol-gel method could well im-

†To whom correspondence should be addressed.
E-mail: qiulinzhang_kmust@163.com

mobilize the Ni species into the porous framework of the Al_2O_3 aerogel to well disperse Ni species and prevent the sintering of Ni nanoparticles with the increase of the activities and coking-resistance for DRM. Highly active and stable MgO-coated Ni catalysts reported by Kim et al. [19] were fabricated via atomic layer deposition and there was negligible deactivation during long-term DRM reaction. Wang et al. [20] used an evaporation-induced self-assembly method to prepare Ni-Al_2O_3 catalysts with high dispersion and small particle size, which impeded the aggregation of the Ni sites at high temperature. However, these are complex processes of preparation that may not be applied for industrial production in large scale. Another synthetic route, homogeneous precipitation, has been proposed to prepare supported catalysts of high dispersion and small particle size especially for silica-supported metal catalyst. As a simple method modified on the base of precipitation, it slowly deposits its precursor species on the support so that the uniformly distributed metal particles and strong metal-support interaction can be obtained [21]. Additionally, this process affords reproducibility, which makes sense for industrial operation [22]. Burattin et al. [22-25] used this method to successfully prepare Ni/SiO_2 and Cu/SiO_2 samples with high loading, good dispersion and strong metal-support interaction. Similarly, the catalyst derived from the precipitation process was reported to show excellent activity in the hydrogenation of naphthalene according to the Rodolfo Gómez-Reynoso et al. [26].

We prepared Ni/SBA-15 catalyst by homogeneous precipitation and studied its catalytic performance for DRM. Up to now, no relevant research has been reported on the Ni/SBA-15 prepared by this kind of method to apply in DRM. The catalyst was characterized by N_2 adsorption-desorption, XRD, H_2-TPR, TEM and TG-DSC. Moreover, the structural properties, Ni particles dispersion and the degree of coke and sintering of the catalysts were also further studied.

EXPERIMENTAL

1. Preparation

The synthesis procedure of the SBA-15 referred to the method described in the literature and was given in detail [27]. 4 g of P123 was weighed and solved in 30 mL of deionized water and 120 mL of aqueous hydrochloric acid (1.6 M HCl), then the suspension was stirred at 40 °C for 2 h until P123 was completely dissolved. 5 g tetraethyl orthosilicate was dropwise added into the above solution; after stirring for 24 h the white liquid was transferred to the high-pressure autoclave for crystallization under the condition of 100 °C for 24 h. Subsequently was the filtration with deionized water washing for three times. After drying overnight, the as-product was calcined in muffle furnace at 550 °C for 6 h, and the resulting white powder was SBA-15.

The Ni/SBA-15 catalyst was prepared by homogeneous precipitation. The preparation process consulted the description in literature [23]. First, 200 mL mixed solution ($n(Ni(NO_3)_2{\cdot}6H_2O) : n(CO(NH_2)_2) : n(HNO_3)=7 : 21 : 1$) was prepared and 1.52 g of SBA-15 was added into the above solution (Ni/Si molar ratio=0.06). Next, the mixture was placed in a water bath heated to 90 °C and the precipitation started after 3 min stabilization. By 4 h of agitation, the heating was stopped when the pH of the solution was ~7. After the temperature naturally cooled to 20-25 °C, the compound was filtered by deionized water. Then the residue was washed for three times by 20 mL deionized water with stirring at 50-60 °C for 10 min each time. The final product was dried at 90 °C for 24 h and calcined at 550 °C for 6 h. The resulting solid powder was the Ni/SBA-15, defined as Ni-HP catalyst.

As a comparison, Ni/SBA-15 with the same Ni loading was prepared by the incipient impregnation method. A certain amount of nickel nitrate was dissolved in deionized water and 1 g SBA-15 was added to stir for 1 h followed by 1 h standing. After that, the mixture was heated at 60 °C for 4 h and then increased to 70 °C for 1 h. The resulting solid powder was dried overnight in an oven and then heated in an air atmosphere at 550 °C for 4 h calcination. Ultimately, Ni/SBA-15 prepared by impregnation method was obtained and denoted as Ni-IM catalyst. The actual content of nickel in the Ni-HP and Ni-IM catalysts was 5.47 wt% and 5.46 wt% (ICP), respectively.

2. Characterization

The specific surface area and pore structure of the catalysts were measured on a Micromeritics TriStar II3020 physical adsorbent apparatus. About 0.2 g sample was pre-degassed at 300 °C for 4 h before the measurement of N_2 adsorption-desorption at −196 °C. Barrett-Emmett-Teller (BET) and Barrett-Joyner-Halender (BJH) desorption were used to calculate the specific surface area and pore volume of the samples.

The hydrogen-programmed temperature reduction (H_2-TPR) was performed on a fixed-bed micro-quartz, and 0.1 g catalyst was placed in the reactor for 40 min activation under N_2 atmosphere. The catalyst was heated to 400 °C at the rate of 8 °C/min from room temperature and cooled below 100 °C. Then the measurement was carried out along with the temperature rising to 800 °C of 8 °C/min rate under the condition of H_2/Ar (30 mL/min), and the hydrogen signal was detected by thermal conductivity detector (TCD).

X-ray diffraction (XRD) was conducted on a Bruker D8 Advance apparatus employing Cu Kα radiation (λ=0.15406 nm) over a 2θ scanning range of 10-80° with rate of 6°/min. The primary crystallite size of Ni was calculated by the Scherrer equation:

$$D_{Ni}=\frac{0.89\lambda}{\beta\cos\theta}$$

where λ is the X-ray wavelength corresponding to Cu-K radiation (0.15406 nm), β is the full-width (in radians) of the diffraction peak at the half maximum height (FWHM) of the Ni (111) reflection and θ is the Bragg diffraction angle of corresponding peak.

Transmission electron microscopy (TEM) analysis was carried out on a Tecnai G^2 TF30 S-Twin equipment produced by FEI Company of Netherlands with a dot resolution of 0.205 nm, a line resolution of 0.102 nm, an accelerating voltage of 300 KV and the magnification of 2000-1000000 X.

TG-DSC measurement was used to analyze the amount of carbon deposition and the types of coke by TA Q600 Thermogravimetric Analyzer with DSC Q2000 Differential Scanning Calorimeter. The samples were heated under air atmosphere from room temperature to 900 °C at the rate of 10 °C/min.

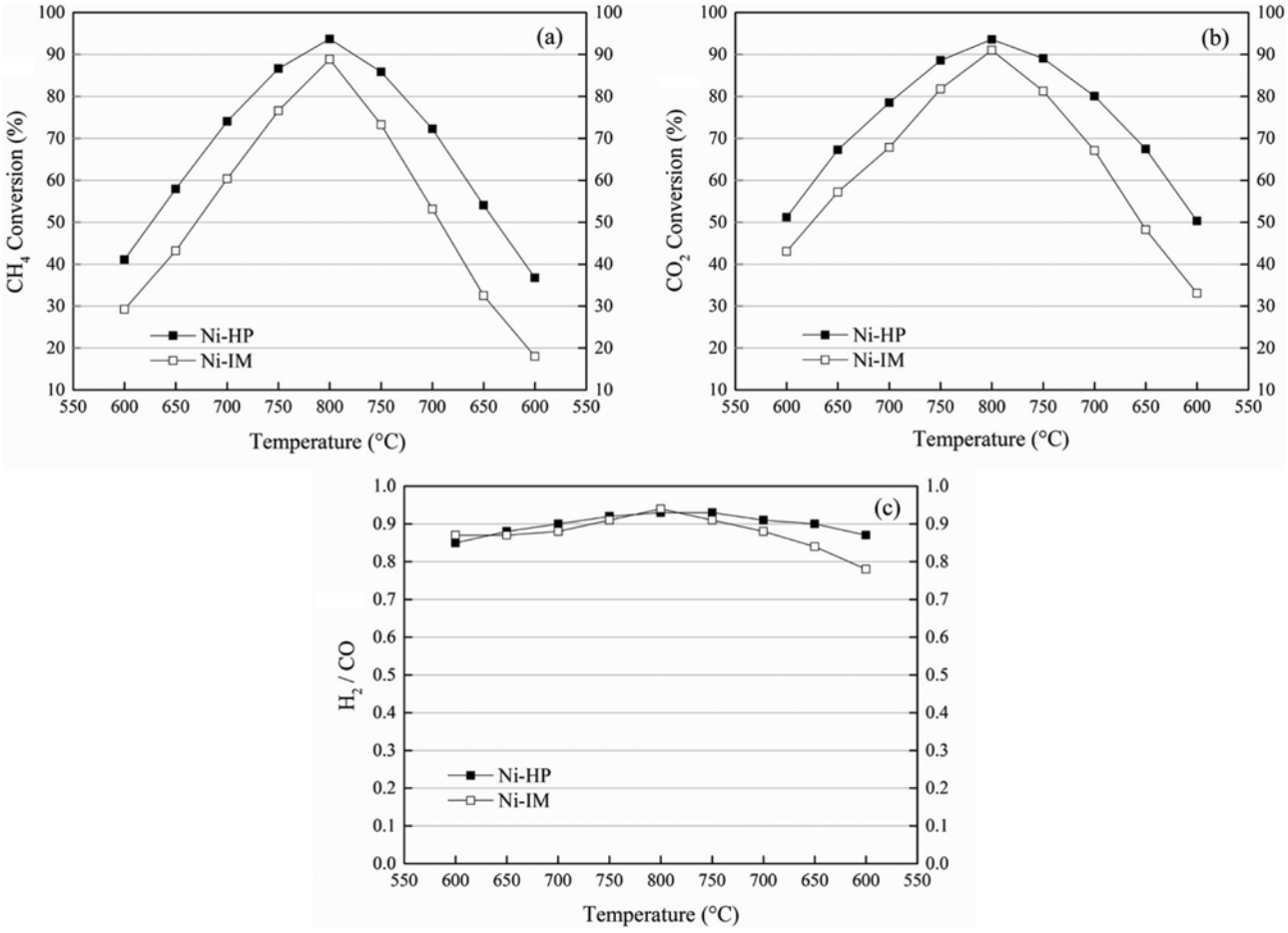

Fig. 1. Initial catalytic activity of the catalysts for dry reforming of methane. (a) CH_4 conversion; (b) CO_2 conversion; (c) H_2/CO (Reaction conditions: m=50 mg, V_{CH4} : V_{CO2}=1, GHSV=36,000 mL/(h·g)).

Raman spectroscopy was conducted on a Renishaw in via microscopic Raman spectrometer equipped with a Leica PL Fluotar 50× objective and Leica microscopy system. 514 nm solid-state laser was used and Raman spectrum was calibrated using a silicon wafer peak at 520.6 cm^{-1} before the measurement. All samples were analyzed under atmosphere without pretreatment.

Inductively coupled plasma optical emission spectrometry (ICP-OES) was adopted to measure the actual content of nickel in the fresh catalysts by the PROFILE SPEC(ICP) equipment (Leeman Labs, Inc.).

3. Catalytic Test

The catalyst activity was evaluated in a micro-fixed-bed quartz tube reactor (i.d.=6 mm) under atmospheric pressure with a catalyst dosage of 50 mg (40-60 mesh). Before the measurement, the catalyst was reduced by H_2 at 700 °C for 1 h and then the reaction gases of CH_4 and CO_2 (V_{CH4} : V_{CO2}=1) with no dilution were introduced. The gas hourly space velocity (GHSV) was 36,000 mL/(h·g), and the reaction temperature was varied from 600 °C to 800 °C. To preliminarily evaluate the stability of the catalyst, the reaction temperature was kept at 800 °C for 4 h and then decreased at a step of 50 °C to 600 °C. After each temperature was maintained for 0.5 h, the resulting effluent was dehydrated by silica gel and analyzed online by a Fuli-9790 gas chromatograph equipped with a TDX-01 packed column and TCD.

RESULTS AND DISCUSSION

1. Catalytic Activity

Fig. 1 depicts the evaluation of the catalytic performance at 600-800 °C of Ni-HP and Ni-IM catalysts in DRM. As mentioned, to initially test the stability at high temperature and the degree of the sintering, these catalysts were performed from 600 °C to 800 °C and maintained at 800 °C for 4 h, then cooled step by step in the test range of 800-600 °C. Generally, the conversions of CH_4 and CO_2 increased with the temperature rising, but the CO_2 conversion was higher than CH_4 conversion and the H_2/CO was lower than the theoretical value of 1, involving the existence of RWGS reaction ($CO_2+H_2 \rightarrow CO+H_2O$) [7]. It is evident that both conversions of CH_4 and CO_2 over Ni-HP catalyst were higher than those of Ni-IM catalyst at all tested temperatures no matter before or after the process of the short stabilization. Remarkably, the catalytic activity of Ni-HP catalyst almost held the same standard from 800 °C to 600 °C, while the Ni-IM catalyst showed apparent deactivation especially returning to 600 °C, with a notable decline of CH_4 and CO_2 conversions from 29.2% and 43.0% to 18.0% and 33.1%, respectively. Although the Ni-IM catalyst still maintained compa-

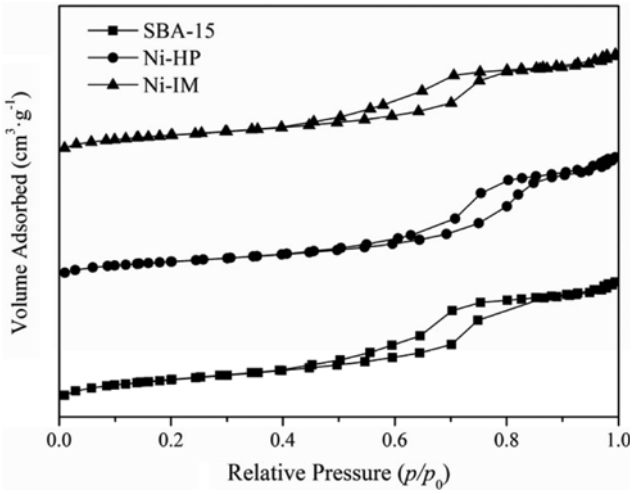

Fig. 2. N_2 adsorption-desorption isotherms of the fresh catalysts.

rable catalytic activity at 750 °C and 700 °C, which was affected by the thermodynamic factor, the sintering resulting from the metal aggregation was irreversible, so the quick deactivation at 650 °C and 600 °C would become more distinct [28]. By comparison, the obvious advantages on the basic activity of Ni-HP catalyst for DRM were found and its superior catalytic performance would be further explained by the following characterization results.

Table 1. BET surface area and pore properties of samples

Sample	Surface area/ $(m^2 \cdot g^{-1})^a$	Average pore diameter/nm^b	Pore volume/ $(cm^3 \cdot g^{-1})^b$
SBA-15	678.6	6.4	0.8
Ni-IM	443.4	7.1	0.7
Ni-HP	405.1	9.5	0.9

[a]Calculated by BET method
[b]Calculated by BJH method

2. The Pore Structure of Catalysts

Fig. 2 shows the N_2 adsorption-desorption isotherms of samples, and the specific pore structure parameters are given in Table 1. All samples have typical IV adsorption-desorption isotherm and H1-type hysteresis loop. The adsorption-desorption isotherm of Ni-IM catalyst is almost unchanged compared with that of the pure SBA-15, indicating that the mesoporous structure of the Ni-IM catalyst was well maintained [29]. Likewise, after loading Ni by homogeneous precipitation, the hexagonal mesoporous structure still remained in the support for Ni-HP catalyst. However, it is interesting, in Table 1, that in spite of the noticeable decline of the specific surface area and slight increase of average pore size observed on both Ni-IM and NI-HP catalysts compared with the support SBA-15, Ni-HP catalyst exhibited a relatively lower specific surface area and larger average pore diameter. This could be presumed that

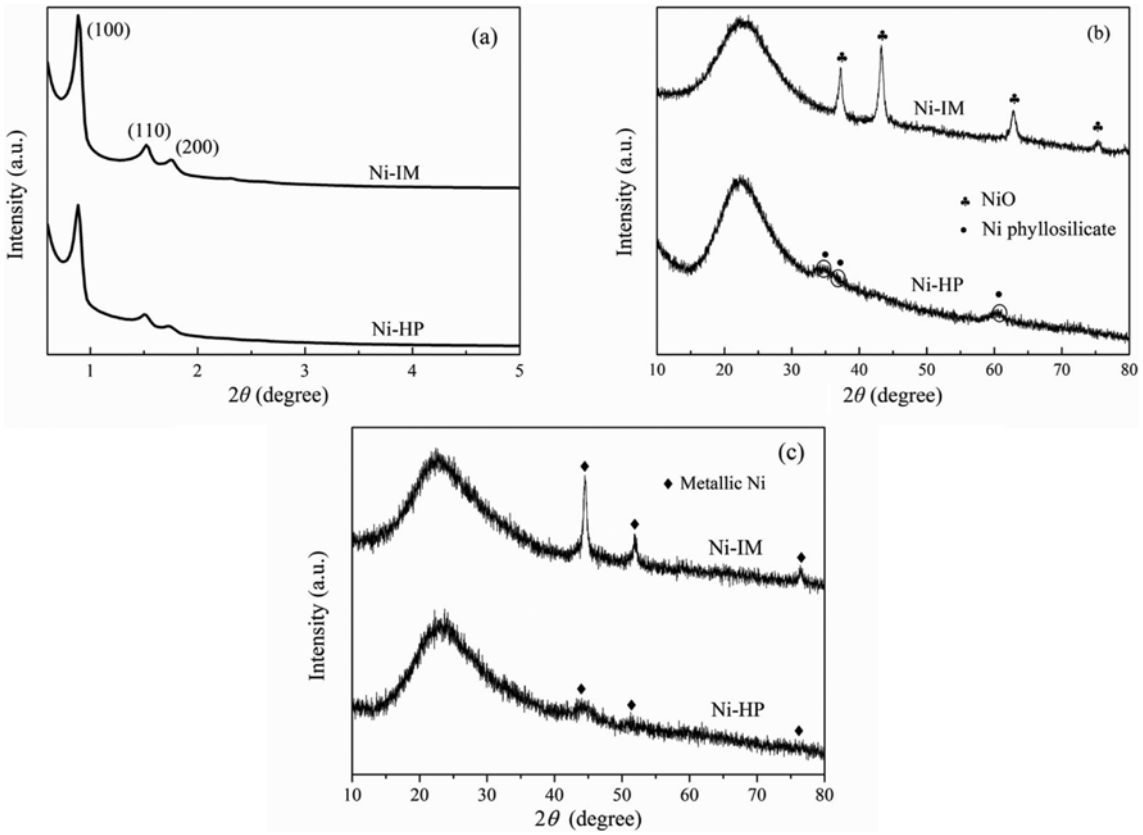

Fig. 3. XRD patterns of catalysts. (a) small angle XRD patterns of fresh catalysts, wide angle patterns of (b) fresh catalysts and (c) reduced catalysts.

the impregnated Ni particles resulted in the blocking of mesoporous, while it is microporous that is jammed during the loading of Ni species by homogeneous precipitation. The nonuniform dispersion and agglomeration of Ni are responsible for the phenomenon of Ni-IM catalyst, but as for Ni-HP catalyst, especially, part of the support was converted into disordered silica and the formation of nickel phyllosilicate during the heat treatment dissolved the silicon wall of sectional support [22-25].

3. XRD Analysis

Ni-HP and Ni-IM catalysts were characterized by X-ray diffraction (XRD) to investigate the existing status of active Ni species and the structural feature of the fresh catalysts. The XRD spectra of the catalysts are shown in Fig. 3. As can be seen in Fig. 3(a), the small-angle XRD patterns of both catalysts are similar to those reported for SBA-15, containing three diffraction peaks at the positions of 2θ=0.8°, 1.5° and 1.8°, which correspond to (100), (110) and (200) reflection, respectively. The intensities of three diffraction peaks for Ni-HP catalyst are relatively weak compared with Ni-IM catalyst, attributed to the destruction of partial pores in the support during the homogeneous precipitation process. The above results suggest that the Ni-HP and Ni-IM catalysts still keep the ordered two-dimensional hexagonal structure of the mesoporous SBA-15 after the introduction of Ni species, same as the results of N_2 adsorption-desorption [30,31].

In Fig. 3(b), both the calcined and fresh catalysts have a broad diffraction peak (2θ=15-31°) belonging to the amorphous SiO_2 [32]. The diffraction peaks of the Ni-IM catalyst in the wide angle XRD at 2θ=37.1°, 43.2°, 62.9° and 75.4° are ascribed to the (101), (012), (110) and (113) reflections of face centered cubic NiO (JCPDS no. 44-1159), respectively, indicating that Ni species mainly exist in the form of NiO. Three relatively weak diffraction peaks (2θ=34.1°, 46.7°, 60.5°) can be found on Ni-HP catalyst in Fig. 3(b), attributed to (200), (202), and (060) reflections of the Ni-phyllosilicate (JCPDS no. 49-1859), of which structure may be ill-formed. Nevertheless, the absence of NiO diffraction peaks means the high dispersion of Ni species in Ni-HP catalyst.

XRD patterns of reduced catalysts were also obtained and presented in Fig. 3(c). For Ni-IM catalyst, three obvious diffraction peaks at 44.6°, 51.9° and 76.5° attributed to (111), (200), (220) crystalline planes of metallic Ni (JCPDS no. 04-0850) were observed in Ni-IM catalyst. The average Ni particle size was determined by using the diffraction peak at 44.6° (111) by Scherrer equation. The calculated results are shown in Table S1. However, in case of Ni-HP catalyst, the diffraction peaks of metallic Ni were quite weak with large width at half height, suggesting the small crystal size and high dispersion in agreement with the XRD results of fresh catalysts. Therefore, it may be not accurate to calculate the crystallite size of metallic Ni by means of the Scherrer equation from such broadened peaks.

4. H_2-TPR Analysis

H_2-TPR was carried out to evaluate the interaction between Ni species and support in the catalysts. It has been reported that the catalyst is more difficult to be reduced and the dispersion of the metal on the catalyst surface is better when the interaction between metal and support is stronger [33]. As shown in Fig. 4, both Ni-HP and Ni-IM catalysts have a weak reduction peak below 300 °C,

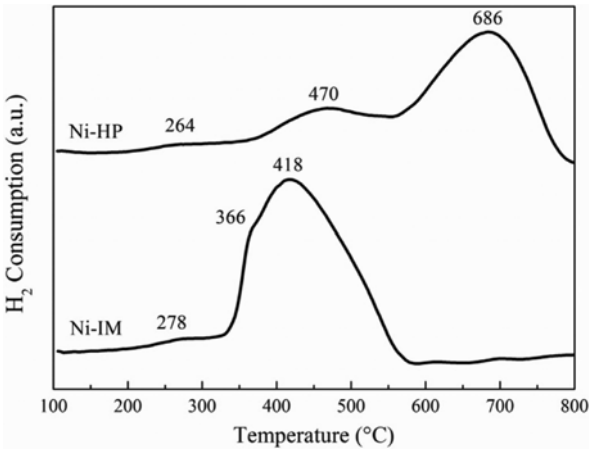

Fig. 4. H_2-TPR profiles of the fresh catalysts.

which is attributed to the reduction of small amount of bulk NiO [3]. And the peaks at 366 °C, 418 °C, and 470 °C are attributed to the reduction of NiO with relatively weak metal-support interaction [34,35]. The third reduction peak of the Ni-HP catalyst is at 686 °C, higher than 550 °C, which should be ascribed to the reduction of nickel phyllosilicate [23]. Due to the stability of Ni-O-Si bond, the metal-support interaction is preeminently enhanced [26]. Comparing the results obtained by H_2-TPR between the two kinds of catalysts, the active composites are mainly in the form of NiO for Ni-IM catalyst, indicating the poor interaction between metal and support. Whereas, Ni species in Ni-HP catalyst exist in the form of nickel phyllosilicate, suggesting a strong metal-support interaction, which is beneficial to the dispersion of active component and could help to improve the anti-sintering performance of the catalyst by suppressing the agglomeration of Ni particles at high temperature in DRM reaction [36].

5. The Stability of Catalysts

Ni-based catalysts for methane dry reforming reaction exhibit good catalytic activity, but the carbon deposition and sintering are likely to occur on the active component during the reaction, leading to a rapid decline in catalytic performance [37]. To explore the catalytic stability, the catalysts prepared by the two methods were exposed to the reactant gases at 700 °C for 100 h. In Fig. 5, even after 100 h reaction, the conversions of CH_4 and CO_2 over Ni-HP catalyst are basically maintained and the ratio of H_2/CO is always kept close to 1, which indicates that Ni-HP catalyst has better catalytic stability. On the contrary, the CH_4 and CO_2 conversions of Ni-IM catalyst sharply decrease from the initial values of 61.7% and 68.7% down to 37.7% and 49.5%, respectively, under the same conditions. Moreover, the ratio of H_2/CO on both catalysts fluctuates in a certain range, due to the alternate reaction of coking and carbon elimination [38]. These results imply that excellent catalytic stability at high temperature can be obtained over Ni/SBA-15 prepared by homogeneous precipitation method. And the reason could be explained by the well-dispersed Ni species and enhanced metal-support interaction, as mentioned above in the results of XRD and H_2-TPR.

6. TEM Analysis

The distribution of Ni particles and morphology of the catalysts

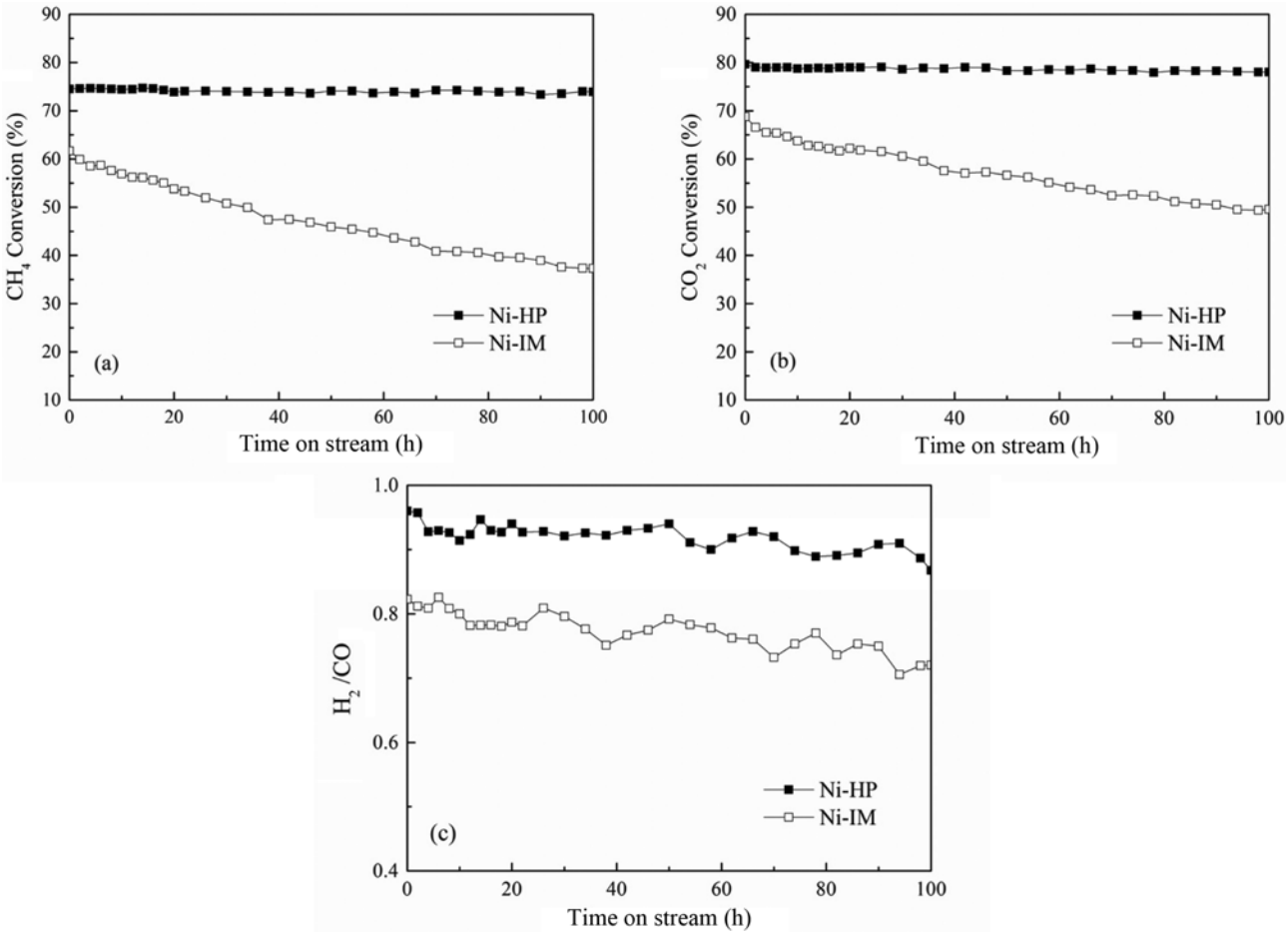

Fig. 5. Stability test of catalysts for 100 h. (a) CH_4 conversion; (b) CO_2 conversion; (c) H_2/CO (Reaction conditions: m=50 mg, T=700 °C, V_{CH4} : V_{CO2}=1, GHSV=36,000 mL/(h·g)).

can be observed by TEM. As shown in Fig. 6(A), although the Ni-IM catalyst remains a good ordered mesoporous channel structure, there are a large number of black regions in Ni-IM catalyst, representing the agglomeration of Ni particles. In contrast, mesoporous structure in Ni-HP catalyst is not maintained as well as Ni-IM catalysts as seen in Fig. 6(B), while some parts of the support are relatively poor due to the dissolution of the silicon wall of partial pores during the heat treatment in the homogeneous precipitation process. As mentioned above in XRD analysis, the intensity of Ni-phyllosilicate peaks is relatively low so that there is no obvious structural feature of plate or needle-type that could be observed in TEM due to the ill-formation of phyllosilicate [39]. The size distribution of Ni particles inserted in Fig. 6(A) for Ni-IM catalyst is rather wide at about 5-15 nm and the average particle size is 11.2 nm. Besides, Ni particles (>25 nm) were unevenly distributed with large size. Considering the 4-6 nm pore size of SBA-15, it can be presumed that the Ni particles are primarily located on the surface of the support instead of entering into the pores. However, in Fig. 6(B), the Ni particle size distribution of the Ni-HP catalyst is mainly concentrated at 2-5 nm and the average particle size is only 3.7 nm, indicating that Ni/SBA-15 prepared by homogeneous precipitation method possesses smaller size of nickel particles and uniform distribution as well. According to the former reports, the smaller particle size could be formed after reduction by H_2 if the metal-support interaction is stronger, which further confirms the presence of strong interaction between the metal and support in Ni-HP catalyst [40,41].

Fig. 6(C) and (D) are the TEM images of the spent catalysts after performing at 700 °C for 100 h. The size distribution of Ni-IM catalyst centralizes at a wide range of 7-25 nm and the average particle size is about 14 nm. Larger Ni particles can be apparently observed in the Ni-IM catalyst as shown in Fig. 6(C), illustrating that the Ni particles move and aggregate together into bigger ones because the Ni particles are not well stabilized in the support channels during the long-time high temperature reaction. On the contrary, Ni particles are highly dispersed in the Ni-HP catalyst and the particle size distribution is still held at around 3-6 nm with the average particle diameter of only 4.7 nm. Therefore, after 100 h reaction at 700 °C, the particle size of Ni-HP catalyst is not evidently increased and the Ni particles are uniformly distributed on the SBA-15 as before. The results indicate that compared with the impregnation method, the catalyst prepared by homogeneous precipitation has the good property of anti-sintering.

Ni-HP catalyst has a stable high-temperature reaction activity owe to its relatively small particle size, uniform distribution and the strong metal-support interaction to stabilize the active nickel spe-

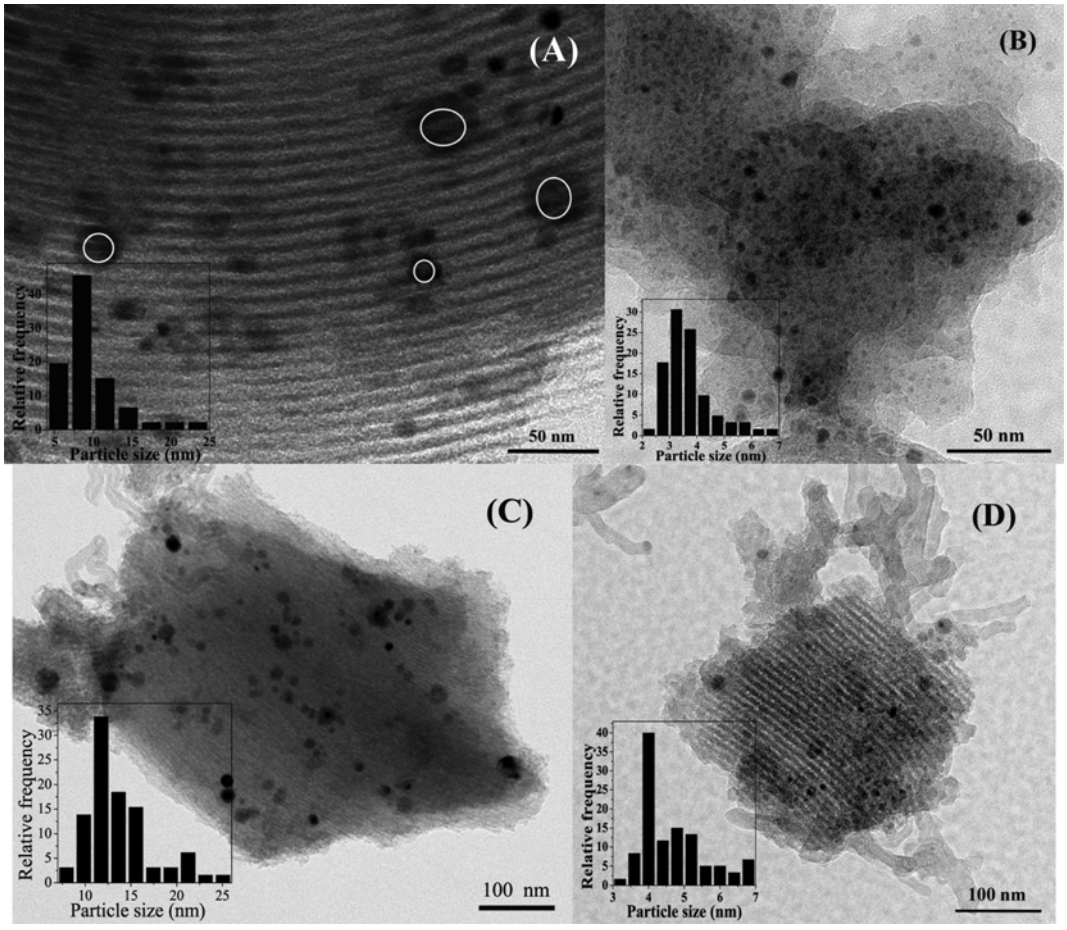

Fig. 6. TEM images of the reduced catalysts (A) Ni-IM, (B) Ni-HP, and spent catalysts after reaction for 100 h at 700 °C (C) Ni-IM, (D) Ni-HP.

cies with improved resistance to sintering. Additionally, the Ni-phyllosilicate, a kind of layered structure, makes Ni^{2+} well immobilized in the support with a good restriction effect and after H_2 reduction the well-dispersed Ni particles are formed [41]. As a result, Ni-HP catalyst could hold stable high-temperature catalytic performance for a long time and get enhanced resistance to sintering.

7. Analysis of Carbon Deposition

TG-DSC was measured to investigate the degree of carbon deposition over the Ni-IM and Ni-HP catalysts after the 700 °C 100 h time on stream DRM reaction. The weight losses of both catalysts involving the combustion of deposited carbon were similar as shown in Fig. 7(a) and Table S1. It suggests that a certain amount

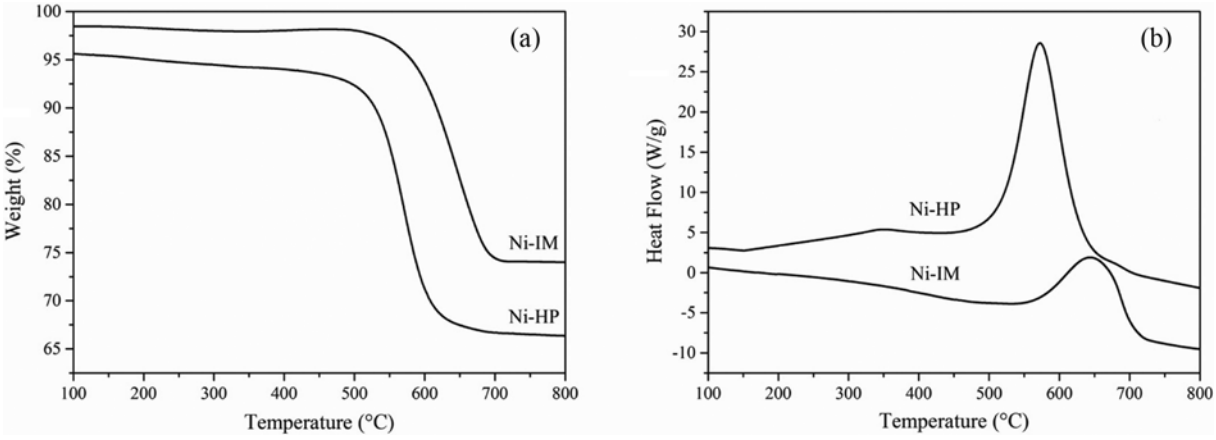

Fig. 7. (a) TG results of spent catalysts, (b) DSC results of spent catalysts after 100 h long-term stability test.

of coke was formed on Ni-IM and Ni-HP catalysts, derived from the decomposition of methane and the disproportionation of carbon dioxide [1]. Different temperatures at which the coke could be burnt indicate the different types of carbon deposition. On the basis of previous literature, there are three kinds of carbon which could be formed during the process of DRM for Ni-based catalysts, known as C_α, C_β, C_γ, respectively. The most easily being oxidized C_α is amorphous carbon, assigned to the temperature range of 150-350 °C. C_β, as a common carbon type, is shaped in the structure of filament with or without Ni particles inside and can be found around 530-600 °C. While, the carbon oxidized at higher than 600 °C is designated to layered encapsulating C_γ, a kind of inert graphite carbon that is responsible for the deactivation of the catalyst [42,43]. Hence, in Fig. 7(b), the sharp peak observed at 570 °C of Ni-HP catalyst can be ascribed to the filamentous carbon whereas the relatively low peak of 640 °C is considered to be the inactive graphite carbon in the Ni-IM catalyst. And this is also confirmed by the TEM (Fig. 6(D) and Fig. S1) that for Ni-IM catalyst, the Ni particle is surrounded by the closed layers of graphite carbon, signifying the deactivation of the active site. Whereas, on account of the reported base-growth mechanism and the results obtained in the long-term activity test, the filamentous carbon mainly grows in the entrance of pore channel around the Ni-HP catalyst with the Ni particles at the bottom [44] (Fig. S2). They could not drive the Ni particles away off the support due to the existing strong interaction and have negligible effect on the activity that Ni particles still act as the catalytic role. However, the situation is totally different for Ni-IM catalyst that carbon deposited as many graphite layers to encapsulate the Ni particles, resulting in the overlap on the active sites [43]. Therefore, the Ni-HP catalyst still holds stable conversions after the time on stream measurement with the presence of comparable amount of carbon deposition as the Ni-IM catalyst.

The presence of carbon deposition in spent catalysts is also revealed by the Raman spectroscopy to obtain more information on the properties and structure of coke. For both catalysts, two obvious peaks were observed at ~1,346 cm^{-1} (D band) and ~1,580 cm^{-1} (G band). The D band is deemed to be the disorder induced by structure imperfection existing in defective carbonaceous species. The G band is associated with graphite carbon, involving the symmetry and order degree [45,46]. The intensity ratio of two bands (I_G/I_D) was adopted to reflect the structured or crystalline/graphitization level of carbonaceous species [47,48], as displayed in Table S1. Although the amount of carbon deposition on the two catalysts is close to each other or that of Ni-HP is even slightly more than Ni-IM, crystalline degree (I_G/I_D) of carbon deposition on spent Ni-HP (0.87) is lower than that of spent Ni-IM (1.36). The result further demonstrates that the carbon deposited on Ni-HP is mainly amorphous and disordered, which takes up a large proportion in the total amount of the carbon deposition. While, the coke presents high graphitization level on Ni-IM, accounting for the cover and encapsulation of the active sites to deactivate. The analysis of Raman spectra is well in accordance with the TG-DSC results.

Combining the TG-DSC and Raman characterization results, it can be concluded that the catalytic performance depends less on the amount of carbon deposition but more on the types of carbon species [49]. Albeit a little higher amount of coke than Ni-IM, Ni-HP maintains stable activity and generates just more filamentous carbon which is active and amorphous, as displayed in Fig. S2. On the one hand, the strong metal-support interaction induced via homogeneous precipitation hinders the deactivation of Ni particles caused by the growth of carbon. On the other hand, filamentous carbon itself has almost no impact on the Ni active sites. Similar observations are shown in previous publications [50-52]; the filamentous carbon has minor influence on the catalytic performance as the particles could keep cleanliness of their active surface and even exposed Ni sites sticking to the carbon should be catalytically active in the reaction. Moreover, proper amount of active carbon benefits to prevent the deactivation to some extent [51,52]. As a result, Ni-HP catalyst could retain steady activity in the long-term stability test and not be affected by the produced active carbon species.

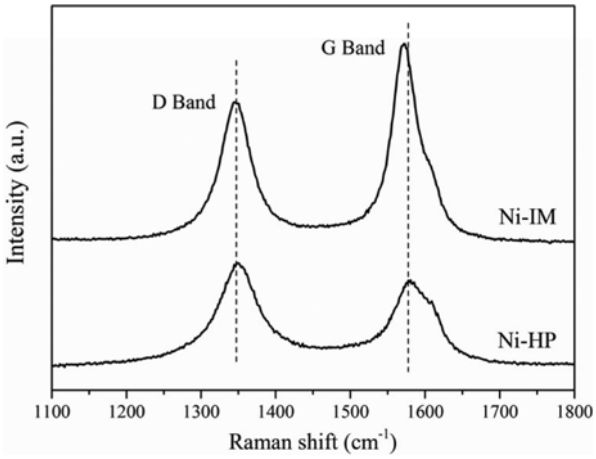

Fig. 8. Raman spectra of spent catalysts after 100 h long-term stability test.

CONCLUSIONS

Ni/SBA-15 was prepared by homogeneous precipitation method and its catalytic performance in DRM was investigated. The results demonstrated that the catalytic activity of Ni-HP presented no obvious decline after reacting at 700 °C for 100 h. Also, smaller size of Ni particles with high dispersion on the surface of SBA-15 and strong metal-support interaction was found in Ni-HP compared with the catalyst prepared by impregnation. The formation of Ni-phyllosilicate was essential in the process of the homogeneous precipitation, which enhanced the metal interaction with support to improve the stability of Ni-HP catalyst in DRM, especially the resistance to sintering as TEM confirmed. Interestingly, according to analysis of TG-DSC and Raman, a certain amount of carbon deposition was generated on spent Ni-HP, but most of it was active or disorder carbon that had no significant influence on the activity of catalyst. Besides, small particle size and strong metal-support interaction were helpful in reducing the impact of carbon deposition on the Ni active sites. Consequently, homogeneous precipitation method was advantageous in preparing catalyst with stable catalytic performance for dry reforming of methane, as well as anti-sintering and endurance to coke.

ACKNOWLEDGEMENTS

This work was supported by the National Natural Science Foundation of China (No. 21666014).

SUPPORTING INFORMATION

Additional information as noted in the text. This information is available via the Internet at http://www.springer.com/chemistry/journal/11814.

REFERENCES

1. A. Serrano-Lotina and L. Daza, *Int. J. Hydrogen Energy*, **39**, 4089 (2014).
2. M. C. J. Bradford and M. A. Vannice, *Catal. Rev.: Sci. Eng.*, **41**, 1 (1999).
3. S. Damyanova, B. Pawelec, K. Arishtirova, J. L. G. Fierro, C. Sener and T. Dogu, *Appl. Catal. B: Environ.*, **92**, 250 (2009).
4. S. Arora and R. Prasad, *RSC Adv.*, **6**, 108668 (2016).
5. S.-H. Song, J.-H. Son, A. W. Budiman, M.-J. Choi, T.-S. Chang and C.-H. Shin, *Korean J. Chem. Eng.*, **31**(2), 224 (2014).
6. L. Xu, Z. Miao, H. Song and L. Chou, *Int. J. Hydrogen Energy*, **39**, 3253 (2014).
7. L. Xu, H. Song and L. Chou, *Appl. Catal. B: Environ.*, **108-109**, 177 (2011).
8. Z. Liu, J. Zhou, K. Cao, W. Yang, H. Gao, Y. Wang and H. Li, *Appl. Catal. B: Environ.*, **125**, 324 (2012).
9. L. Mo, K. K. M. Leong and S. Kawi, *Catal. Sci. Technol.*, **4**, 2107 (2014).
10. C. E. Daza, J. Gallego, F. Mondragón, S. Moreno and R. Molina, *Fuel*, **89**, 592 (2010).
11. D. Liu, X.-Y. Quek, H. H. A. Wah, G. Zeng, Y. Li and Y. Yang, *Catal. Today*, **148**, 243 (2009).
12. A. J. Van Dillen, R. J. A. M. Terorde, D. J. Lensveld, J. W. Geus and K. P. De Jong, *ChemInform*, **34**, 257 (2003).
13. M. H. A. Shiraz, M. Rezaei and F. Meshkani, *Korean J. Chem. Eng.*, **33**(12), 3359 (2016).
14. X. Li, D. Li, H. Tian, L. Zeng, Z. J. Zhao and J. Gong, *Appl. Catal. B: Environ.*, **202**, 683 (2017).
15. C. Wang, N. Sun, N. Zhao, W. Wei and Y. Zhao, *Catal. Today*, **281**, 268 (2017).
16. Z. Liu, J. Zhou, K. Cao, W. Yang and H. Gao, *Appl. Catal. B: Environ.*, **125**, 324 (2012).
17. Q. Zhang, T. Wu, P. Zhang, R. Qi, R. Huang, X. Song and L. Gao, *RSC Adv.*, **4**, 51184 (2014).
18. X. Zhao, Y. Cao, H. Li, J. Zhang, L. Shi and D. Zhang, *RSC Adv.*, **7**, 4735 (2017).
19. M. G. Jeong, S. Y. Kim, D. H. Kim, S. W. Han, I. H. Kim, M. Lee, Y. K. Hwang and Y. D. Kim, *Appl. Catal. A: Gen.*, **515**, 45 (2016).
20. X. Fang, C. Peng, H. Peng, W. Liu, X. Xu, X. Wang, C. Li and W. Zhou, *ChemCatChem*, **7**, 3753 (2015).
21. G. L. Bezemer, P. B. Radstake, V. Koot, A. J. Van Dillen, J. W. Geus and K. P. De Jong, *J. Catal.*, **237**, 29 (2006).
22. P. Burattin, M. Che and C. Louis, *J. Phys. Chem. B.*, **103**, 6171 (1999).
23. P. Burattin, M. Che and C. Louis, *J. Phys. Chem. B.*, **101**, 7060 (1997).
24. P. Burattin, M. Che and C. Louis, *J. Phys. Chem. B.*, **102**, 2722 (1998).
25. P. Burattin, M. Che and C. Louis, *J. Phys. Chem. B.*, **104**, 10482 (2000).
26. R. Gómez-Reynoso, J. Ramírez, R. Nares, R. Luna and F. Murrieta, *Catal. Today*, **107-108**, 926 (2005).
27. D. Zhao, J. Feng, Q. Huo, N. Melosh, G. H. Fredrickson, B. F. Chmelka and G. D. Stucky, *Science*, **279**, 548 (1998).
28. J. A. Moulijn, A. E. Van Diepen and F. Kapteijn, *Appl. Catal. A: Gen.*, **212**, 3 (2001).
29. R. Srivastava, D. Srinivas and P. Ratnasamy, *J. Catal.*, **233**, 1 (2005).
30. M. E. Gálvez, A. Albarazi and P. Da Costa, *Appl. Catal. A: Gen.*, **504**, 143 (2015).
31. S. He, S. He, L. Zhang, X. Li, J. Wang, D. He, J. Lu and Y. Luo, *Catal. Today*, **258**, 162 (2015).
32. A. M. Gadalla and B. Bower, *Chem. Eng. Sci.*, **43**, 3049 (1988).
33. C. Zhang, H. Yue, Z. Huang, S. Li, G. Wu, X. Ma and J. Gong, *ACS Sustain. Chem. Eng.*, **1**(1), 161 (2013).
34. N. Wang, W. Chu, T. Zhang and X. S. Zhao, *Int. J. Hydrogen Energy*, **37**, 19 (2012).
35. Y. H. Yang, S. Lim, G. A. Du, Y. Chen, D. Ciuparu and G. L. Haller, *J. Phys. Chem. B.*, **109**, 13237 (2005).
36. J. H. Lee, K. Y. Koo, U. H. Jung, J. E. Park and W. L. Yoon, *Korean J. Chem. Eng.*, **33**(11), 3115 (2016).
37. K. Tomishige, Y.-g. Chen and K. Fujimoto, *J. Catal.*, **181**, 91 (1999).
38. L. Xu, Z. Miao, H. Song, W. Chen and L. Chou, *Catal. Sci. Technol.*, **4**, 1759 (2014).
39. X. Y. Gao, K. Hidajat and S. Kawi, *J. CO_2 Util.*, **15**, 146 (2016).
40. S. Uchiyama, Y. Obayashi, T. Hayasaka and N. Kawata, *Appl. Catal.*, **47**, 155 (1989).
41. Q. Zhang, M. Wang, T. Zhang, Y. Wang, X. Tang and P. Ning, *RSC Adv.*, **5**, 94016 (2015).
42. Z. L. Zhang and X. E. Verykios, *Catal. Today*, **21**, 589 (1994).
43. W. Yang, H. Liu, Y. Li, J. Zhang, H. Wu and D. He, *Catal. Today*, **259**, 438 (2016).
44. L. Zhou, L. Li, N. Wei, J. Li and J.-M. Basset, *ChemCatChem.*, **7**, 2508 (2015).
45. X. Zhao, H. Li, J. Zhang, L. Shi and D. Zhang, *Int. J. Hydrogen Energy*, **41**, 2447 (2016).
46. X. Zhao, Y. Cao, H. Li, J. Zhang, L. Shi and D. Zhang, *RSC Adv.*, **7**, 4735 (2017).
47. W. Yang, H. Liu, Y. Li, J. Zhang, W. Hao and D. He, *Catal. Today*, **259**, 438 (2016).
48. W. Yang, H. Liu, Y. Li, H. Wu and D. He, *Int. J. Hydrogen Energy*, **41**, 1513 (2015).
49. H. Fei, W. Rui, Y. Chao, H. Driss, C. Wei and Z. Hui, *J. Energy Chem.*, **25**, 709 (2016).
50. S. Yasyerli, S. Filizgok, H. Arbag, N. Yasyerli and G. Dogu, *Int. J. Hydrogen Energy*, **36**, 4863 (2011).
51. N. Wang, C. Wei, T. Zhang and X. S. Zhao, *Int. J. Hydrogen Energy*, **37**, 19 (2012).
52. D. Liu, X. Y. Quek, H. A. W. Hui, G. Zeng, Y. Li and Y. Yang, *Catal. Today*, **148**, 243 (2009).